May 2019

PEPpy: A tool to generate bacterial peptidoglycan scaffolds for coarse-grained simulations

Xichen Xu
Syracuse University

ABSTRACT

Peptidoglycan (PG), also known as murein, is an essential component in both Gram-positive and Gram-negative bacteria. However, even if the chemical structure has been well-known for long, the great tertiary structure remains not clear due to its variability and complicated cross-link mechanism. And it inevitably raises the huge challenge for computational simulations. Against the background, here we present a method for building a solvated peptidoglycan system at coarse-grained level as required. The method is named *PEPpy*, which represents a Peptidoglycan python code. It reads in the user's parameters in sequence and automatically generates a topological file and a structure file in the meantime. With these files generated, molecular dynamics simulations and a series of analyses can be easily performed afterwards.

PEPpy: A tool to generate bacterial peptidoglycan scaffolds for coarse-grained simulations

by

Xichen Xu

B.S., University of Science and Technology of China, 2016

THESIS

Submitted in partial fulfillment of the requirements for the degree of

Master of Science in Chemical Engineering

Syracuse University

May 2019

ACKNOWLEDGMENTS

I would like to express my sincere gratitude to my advisor Dr. Shikha Nangia. Thank you for giving me the opportunity to join the Nangia Research Group and conduct the research that I am interested in. It has been my great honor to be a part of it. Thanks for your patience, understanding and academic instructions all the way.

My appreciation also goes to all the group members in the lab. It was really helpful to have someone who have so much knowledge and experiences when I was new to this field. Jerome, Huilin and Nandhini: thanks for your guidance and instruction in the very beginning that led me to learn necessary skills in computational simulation. Special thanks to Huilin, you were always there to help whenever I encountered problems in the modeling process. Nandhini, thanks for the troubleshooting of my coding. The assistance from you all was priceless.

During the two and a half years in Syracuse, I have harvested so many friendships that I will treasure forever. Zhen, you are such a considerable guy. Thank you for being my roommate and accepting my flaws all the time. Jiachen and Chen, thanks for always being there for me.

The most special thanks goes to my parents. Mom and dad, I know I can always count on you whenever I am in trouble. Thanks for watching my back and giving me support in all my life's journey.

Table of Contents

LIST OF FIGURES

LIST OF TABLES

CHAPTER 1

INTRODUCTION

1.1 Background

1.1.1 Function and Content of Peptidoglycan. Peptidoglycan (PG) is an important structural component of the bacterial cell and is found in the cell envelope of almost all Gram-positive and Gram-negative bacteria. It protects the cell from the hostile surroundings, and provides mechanical support by resisting the changes in osmotic pressure of the cell[1, 2]. In Gram-negative bacteria, PG layer is approximately 2-3 nm thick and is flanked by an inner phospholipid bilayer and a highly charged lipopolysaccharide-rich outer membrane[3-6]. In Gram-positive bacteria, PG layer is usually 20−100 nm in thickness[6]; in *Staphylococcus aureus* specifically, the PG layer is about 20−40 nm thick[7, 8].

1.1.2 Chemical Structure. The chemical structure of PG comprises three main components-a sugar backbone, a peptide stem, and a short peptide bridge structure. The disaccharide of one basic unit in PG of all types consists of two glucose molecules, N-acetylglucosamine (NAG) and N-acetylmuramic acid (NAM)[2, 5, 7-9]. Differences mainly exist in the composition of the peptide stems and the bridge structures. For instance, FemX mutant of *Staphylococcus aureus* does not have bridge structures in its PG scaffold[9]. In *S. aureus* typically, the stem connected to NAM is a pentapeptide, composed of L-alanine, D-iso-glutamine, L-lysine, and two D-alanine residues (Figure 1), and the bridge structure consists of five glycine residues and can form a cross-link with the adjacent peptide stem [10, 11]. Then the whole PG scaffold is formed by the accumulation of the small PG repeat units through two enzymatic processes, one is to form the glycosidic bonds between disaccharide units and the other is to form the cross-links between the neighboring peptide stem and bridge structure of another NAG-NAM chain.[12, 13]

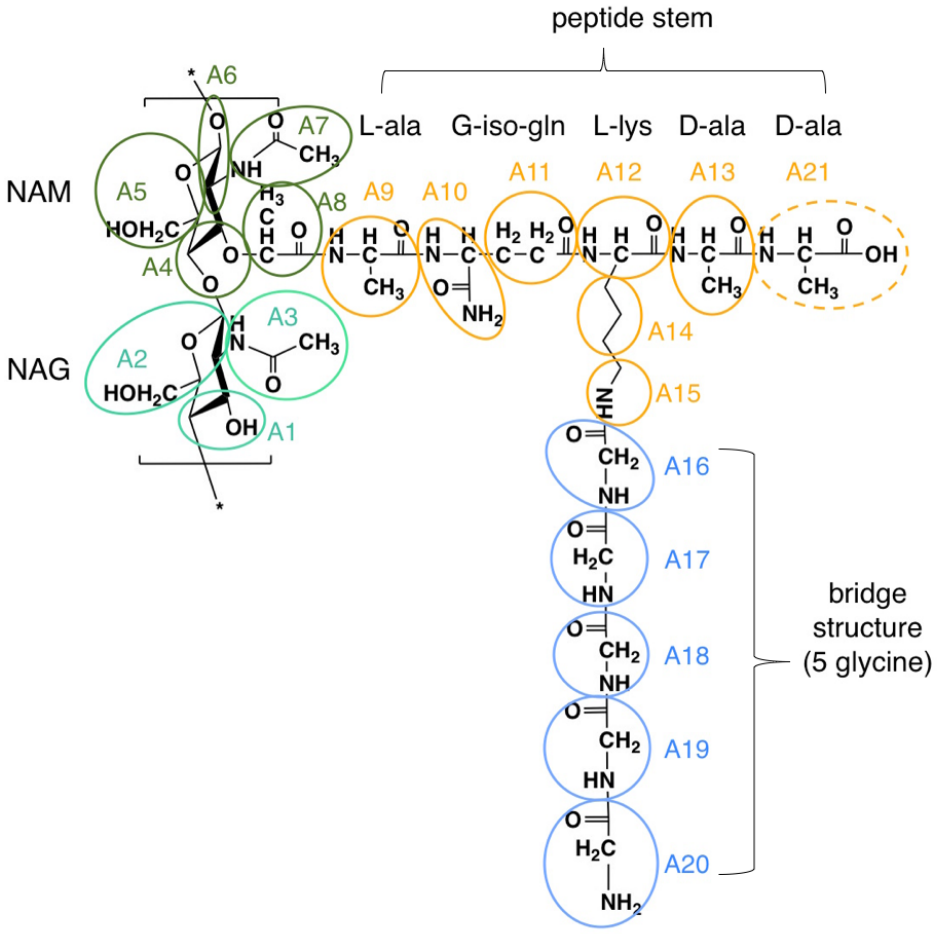

Figure 1. Chemical structure and coarse grain mapping scheme of S. aureus PG repeat unit. The disaccharide head group compose of NAG (light green) and NAM (dark green) and a pentapeptide stem (orange) and pentapeptide bridge (blue) structure. The edged D-alanine of the unit in dashed circle (A21) only exists when the stem is not cross-linked to the bridge of another unit.

1.1.3 3-dimensional PG Structure. For the 3-dimensional PG structure of Gram-positive bacteria, even if the chemical composition has been well-authenticated for long, the complex cross-linked structure in a whole is still greatly not clear due to its large size, variability and complexity. Therefore, traditional methods that serve to investigate structures such as solution-state NMR and X-ray diffraction analysis are not applicable in this situation. And though imaging techniques such as atomic force microscopy or cryoelectron tomography have already

been applied to research in the bacterial peptidoglycan and achieved great success in understanding the physical arrangement of peptidoglycan in Gram-negative bacteria[14-17], they obtained few achievements in investigating Gram-positives for their thick PG scaffolds.

Using solid-state NMR, Kim et al. showed that in *S. aureus* PG forms a three-dimensional lattice with a helical 4-fold axial symmetry[10]. Figure 2 shows when disaccharides are connected, the peptide stem of the successive PG will rotate 90° relative to the stem of the previous PG unit, thus four consecutive PG units are going to form one period in the long glycan strand. In addition, cross-links are able to generate in all directions with the neighboring strands in this configuration.

1.1.4 Previous Computational Simulation Researches. So far, seldom has the computational technique, molecular dynamics simulation, which has been widely used to investigate large and complex models such as bacterial membrane systems [18-22], been applied to study PG. Because compared to membrane systems, PG scaffolds have the more complicated connecting mechanism and irregular configuration.

One early research of bacterial cell wall using simulation techniques conducted by Gumbart et al.[23] was focused on the PG structure of *Escherichia coli*, one common kind of Gram-negative bacteria at the atomistic level. In the work, they developed the atomistic PG model in a circumferential configuration randomly and simulated it to study and characterize several mechanical properties such as elasticity, thickness and pore size. Another simulation research of PG conducted by Samsudin et al.[24, 25], also at the atomistic level, was focused on *E. coli* as well, trying to examine the relationship between the length of *Braun's Lipoprotein* and the distance from PG layer to the bacterial outer membrane.

However, no research has been conducted for Gram-positive bacterial PG systems at the coarse-grained level up to now. Although atomistic simulations provide full details of each atom accurately, it is not affordable for large systems such as the Gram-positive Peptidoglycan scaffolds in particular for a large time-scale simulation. Therefore, our work was trying to depict the 3-dimensional PG model of Gram-positive *S. aureus* through generating the PG structure by a specific code and operating molecular dynamics (MD) simulations in the following.

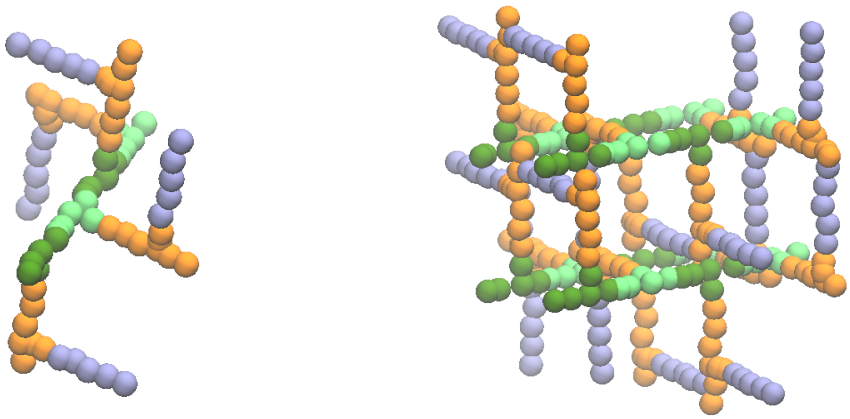

(a) *(b)*

Figure 2. Peptidoglycan single strand and lattice arrangement. (a) Single glycan strand showing disaccharide backbone (green and lime beads) with peptide stems (orange beads) and cross-linking peptide bridges (ice blue beads). (b) Four cross-linked glycan strands in PG lattice.

1.1.5 Coarse-grained Simulation. As is mentioned, the Gram-positive *S. aureus* PG scaffold is relatively too large a system to run MD simulations at atomistic scale for microsecond timescales. Consequently, the next hierarchical coarse-grained (CG) modeling approach aiming at simulations of simplified representation of large systems is introduced to molecular dynamics[26]. Applied to a variety of MD simulations, such as into lipids and proteins[27-32], it

has proven to be a useful method to lengthen the time scales, giving the chance to investigate lager and more complex models through MD and making it possible to require the standard of characterization compared to atomistic models[26, 33]. Therefore, CG mapping is adopted to model the PG scaffold architecture.

1.2 Motivation

Against all the background, we intended to develop a method to investigate the Gram-positive PG architecture through a computational way. The main task of the project was the code *PEPpy* (Peptidoglycan python) for generating the solvated 3-dimensional peptidoglycan lattice system. A coarse-grained PG repeat unit was formed in advance and sent into the script via the topology file. Users are asked to input variables including the sizes and cross-linking ratios that they would like the model to occupy. The coordinate GRO file and the topological ITP file of the whole model could be automatically generated by *PEPpy* in a running time depending on how large the system is. Then molecular dynamics simulations are able to perform in sequence. In addition, various tests were carried out for the models established.

1.3 Workflow

The flowchart of the project is shown in figure 3. The rest of this work is organized as follows. First, a number of approaches that conduct this work are presented in the Methods part. *PEPpy* is described here particularly, providing the background of several pivotal building steps. After that, several examples built by the system are shown which are able to run coarse-grained simulations. In addition, model validations are performed and test of the water diffusion is conducted and presented.

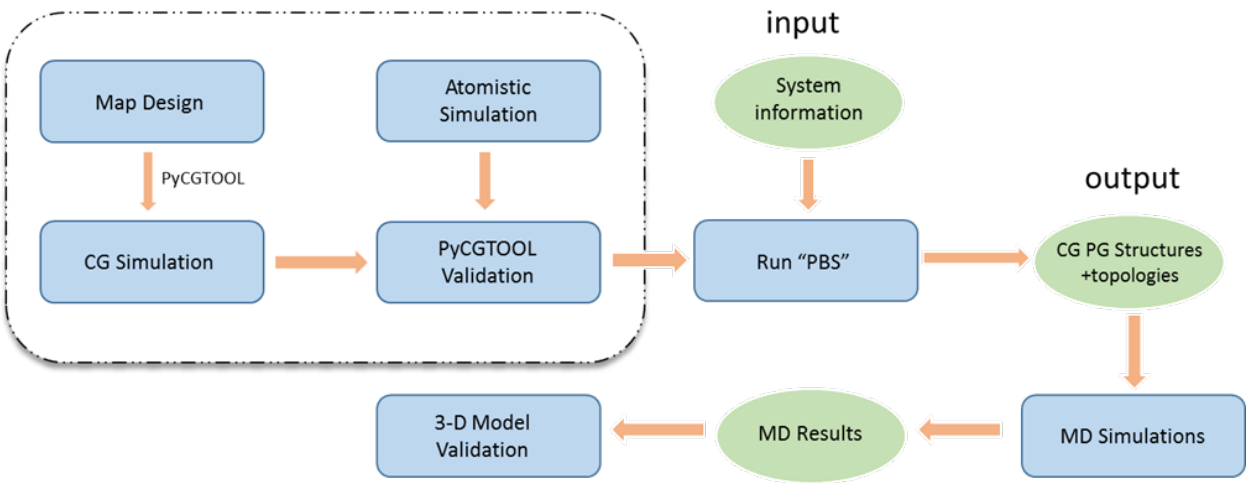

Figure 3. Flowchart of this work. Steps in the dashed box are the preparatory work done in advance. The purpose is to generate the accurate and usable structure and topological file of PG repeat unit that is applicable to Peptidoglycan Building System. Then coarse-grained structures and topologies can be generated by PBS on user's request, which contain the peptidoglycan and solvent (water). Next, energy minimization, position restrained NVT equilibration and NPT equilibration are run in sequence for the completed solvated systems. After that, model validation and other analyses are performed using several tools in GROMACS.

CHAPTER 2

METHODS

2.1. Atomistic simulation

The chemical structure of the PG repeat unit (Figure 1) was drawn with ChemDraw Prime 16.0. The structure was uploaded to the PRODRG Server[34] to build the molecular structure and GROMACS compatible topology files. The GRO file (structure) and ITP file (topology) were then used to run simulations. The atomistic simulations were performed with the MD engine GROMACS, version 5.1.2[35-37], using GROMOS force field, version 54a7[38-41].

Several consecutive simulative steps were involved. The first step was to define the box dimensions and solvate the single molecule. The simulation for the parametrization of PG was able to perform next. The energy minimization adopted the algorithm of the steepest descent minimization. It stopped when the maximum force of all beads in the system were lower than 10.0 kJ/mol/nm within the maximum running time of 0.5 ns. Isothermal-isochoric equilibration run (NVT) was performed for 100 ps with no pressure coupling. Temperature coupling was on at 300 K. The isothermal-isobaric equilibration run (NPT) was performed for 50 ps with pressure at 1 bar and temperature at 310 K. The final step is production MD. It ran for 50 ns at the same pressure and temperature as NPT. Isotropic pressure coupling was used for both NPT and production MD.

2.2. Coarse-grained mapping

Transformed from the atomistic model, the coarse-grained mapping of PG repeat unit was basically based on the MARTINI mapping approach[26, 41-43]. On average one MARTINI bead consists of four heavy atoms, but in a lot of cases two to six heavy atoms can be mapped into a bead for a better systematic organization by assigning specific beads. Details of the coarse-grained mapping into Martini beads are shown in table 1.

Table 1. Details of the coarse-grained mapping of the PG unit into Martini beads

ID	Bead Type	Part of	Bonded to
A1	P1	*NAG*	A2
A2	P4	*NAG*	A3 A4
A3	P4	*NAG*	A2
A4	N0	*NAM*	A2 A5 A8
A5	P4	*NAM*	A4 A6
A6	P2	*NAM*	A5 A7
A7	P3	*NAM*	A6
A8	P3	*NAM*	A4 A9
A9	P4	*L-Ala*	A8 A10
A10	P5	*D-iso-Gln*	A9 A11
A11	P3	*D-iso-Gln*	A10 A12
A12	P5	*L-Lys*	A11 A13 A14
A13	P4	*D-Ala*	A12 A21
A14	C3	*L-Lys*	A12 A15
A15	N0	*L-Lys*	A14 A16
A16	P5	*Gly*	A15 A17
A17	P5	*Gly*	A16 A18
A18	P5	*Gly*	A17 A19
A19	P5	*Gly*	A18 A20
A20	P5	*Gly*	A19
A21	P4	*D-Ala*	A13

The disaccharide backbone was mapped into eight beads from P1 to P4 mostly. For the pentapeptide stem, each amino acid was mapped into one bead except two beads for G-iso-glutamine and three for L-lysine according to the coarse-grained representation of Martini model extension to amino acids by Bradley et al.[44]. In the bridge structure, each glycine was mapped into one bead and assigned type P4. An essential point needs to be emphasized is that bead A21, which is the last bead on the stem shown in a dashed circle in figure 1, is a special bead that not exist in every PG unit in the system due to the cross-linking mechanism. In *S. aureus* PG scaffolds, cross-links are formed between the first D-alanine (A13) on the stem and the N-terminus of the bridge structure of the adjacent PG unit (A20). In the meantime, the peptide bonds between the two D-alanine are hydrolyzed and the second D-alanine at the edge will be

separated from the structure. In brief, the PG unit becomes a 20-bead model when its peptide stem is cross-linked.

2.3. Mapping Validations

In order that the CG model could reasonably replicate the behavior of the atomistic structure, the CG mapping needs to be testified if it is accurate before production simulations. PyCGTOOL was applied to perform the test[45]. A mapping file and a file including bonded terms in readable formats were created according to the specific coarse-grained model, serving as the input files to generate the CG coordinates and the calculated CG topologies by PyCGTOOL. Then the CG molecule was solvated and the CG test simulations for the unit were run using the GROMACS MD simulator within MARTINI force field, version 2.2[26, 27]. The simulations were performed under similar conditions compared to atomistic simulations except the isothermal-isobaric equilibration (NPT) is omitted.

Model validation was performed when both atomistic and CG simulations were completed. The method was to compare the distribution of bond and angle parameters between the results of atomistic simulations and CG simulations[45]. The mean and standard deviations of the bonds and angles were calculated. A small percentage difference of the compared parameters between the simulations would suggest the CG test model to be good enough for the production MD simulations.

2.4. Generation of the desired PG scaffold and solvated system

The major work of this project was to generate the solvated 3-dimensional coarse-grained PG lattice box for simulations. The job was completed by the method we provide called *PEPpy*. It is a code that combines two interactive python scripts, *PEPpy_build* and *PEPpy_solvate*. *PEPpy_build* is literally to generate a coarse-grained PG scaffold in a box with user-determined box size. And the following *PEPpy_solvate* is used to rotate the model for calibration as well as fill the box with water to solvate the PG model. *PEPpy* integrates the two parts together in order to provide a better interactive experience.

2.4.1 Building the 3-D Structure. The *PEPpy* builds the solvated PG system at the coarse-grained level. The *insane* script[46], which mainly deals with the membrane system, was partially used for reference to technically set up the coordinate. The fundamental approach of *PEPpy_build* to generate PG structure is basically setting up a grid with coordinates and adding PG MARTINI beads into specific lattices in sequence. One basic PG repeat unit with 20 beads (bead A21 is not included intendedly) is inserted into the system first. It is fixed at the origin with the disaccharide backbone pointing toward the direction of $+y$, the peptide stem toward $+z$ and the bridge structure toward $-x$. Hence, the orientation as well as coordinates of each bead is fixed for the first PG unit. When *PEPpy* reads in user's input of the box size, the total amount of units this box can hold is calculated and determined. Then *PEPpy_build* follows the helical 4-fold axial symmetry to build a glycan strand along $+y$ direction until the strand reaches the other edge of the box. Next the strand will be replicated along $-x$ direction so that a PG plain is completed at the bottom face of the box. Since the bottom surface is built, the whole 3-

dimensional structure can be set up by replicating the plain along $+z$ direction until reaching the top.

2.4.2 Generating Cross-links. *PEPpy_build* is going to handle with the cross-links after the whole structure is roughly completed. As the cross-linking mechanism is mentioned before, it becomes 20 beads in one PG unit only if its peptide stem has been cross-lined with the adjacent cross-bridge of another unit, that is, if we assume the cross-link reaches 100 percent, all the units are going to have 20 beads, thus not an A21 is required to add into the system. Since a specified cross-link percentage is given, *PEPpy* is able to read in the user's input and add specific number of bead A21 into the system accordingly which are bonded to bead A13 of the PG units randomly. The construction of the 3-D PG structure is then completed.

2.4.3 Topological Information. As the generation of structure file is already completed, a topology file is necessary as well for a system to run MD simulations. It usually lists the atom types of the molecule, bonds, angles and restraints, etc. For coarse-grained beads, the topological information is usually more concise as they are the simplified models to their atomistic counterparts. According to the corresponding coordinate file generated, every bead of PG units in the whole system is assigned a serial number as well as every bond that connects two beads and specific angles, respectively. The information is listed in ITP file.

2.4.4 Alignment and Solvation. When the previous steps accomplished by *PEPpy_build* are almost finished, *PEPpy_solvate* is executed in the following. As long as the 3-dimensional PG model built by *PEPpy_build* is not rigidly aligned horizontally, a rotation is processed around the

axis so that each face of the PG structure becomes parallel to the respective box surface. The final step for the system before performing MD simulations is to fill it with solvent (water). The coarse-grained water molecule is prepared in advance and added into the system with specific amount calculated.

2.4.5 Adding Position Restraints. Periodic boundary conditions (PBC) are frequently applied to molecular dynamics to simulate processes for large systems by using a small unit cell, especially in membrane lipid architecture and protein folding. However, the PBCs in GROMACS do not fit well with PG due to its heterogeneity and complex bonding types. The PG coarse-grained beads at the edge of box are not able to form chemical bonds with beads in adjacent boxes, which may cause the structure to collapse during MD simulations. To overcome this problem, position restraints were applied to the edged beads which should have been bonded so as to simulate the influence of the bonded terms. Position restraints, as the special interactions defined in GROMACS to restrict the motion of a system[35], are harmonic interactions of specified beads with relatively fixed positions when involving coarse-grained models. When the edged beads in the PG structure are selected and restrained, it can to some extent mimic the complete bonded system and avoid intense rearrangements within the structure.

2.5 MD simulations for the coarse-grained PG system

When the CG mapping of the PG repeat unit was tested well for further MD simulations, *PEPpy* was going to receive parameters of the unit to start the building process. To construct the desired PG structure, four variables were needed as input to define the system, three for the definition of

the box dimensions and one for the cross-linking percentage. The building process should take some time, ranging from a few seconds to hours depending on how large the box size was. The system completed was presented by a coordinate file and a topological file when the construction was finished.

The coordinate and topological files generated by *PEPpy* were served as input files for MD simulations. The parameters for each run is quite different from the atomistic simulation. The energy minimization was performed using the algorithm of the steepest descent minimization with a time step of 20 fs and the maximum running time is 2 ns. Isothermal-isochoric equilibration run (NVT) was performed for 20 ns in the time step of 10 fs with two groups, the PG and the solvent. The isothermal-isobaric equilibration run (NPT) was performed 20 μs in the time step of 20 fs. Temperature was set at 310 K for both NVT and NPT. Semi-isotropic pressure coupling in Berendsen barostat was adopted for NPT and the pressure was maintained at 1 bar and temperature at 310 K. Position restraints were exerted on the beads at the edge of the PG structure for NVT and NPT simulations.

2.6. Analysis

The validation of the PG repeat unit has been mentioned before in which PyCGTOOL was applied. Bonded parameters including bond lengths and bond angles were measured with the *gmx_bond* and *gmx_distance* tool in GROMACS when MD simulations were completed. The frequency distributions of bond lengths and angles were calculated by using the xvg files. Then

they were compared to the lengths and angles before the simulation to study the transformation of bonded parameters and the stability of the structure through the simulation.

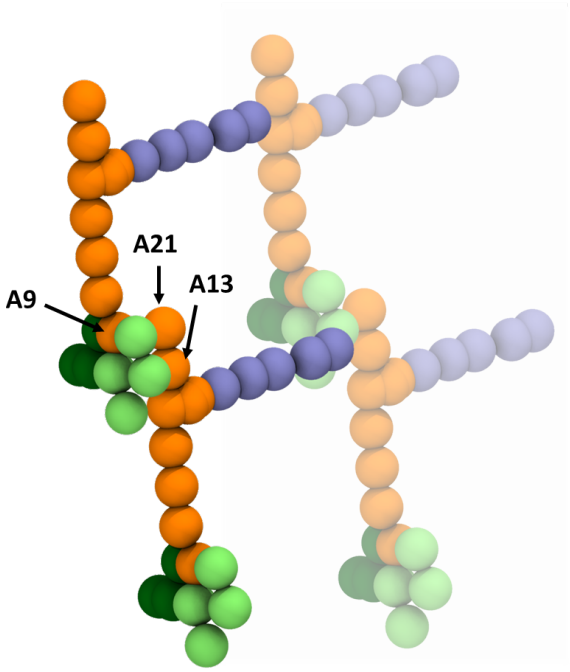

Figure 4. A sketch of a small cross-section of PG structure of S. aureus. Balls in greens represent the glycan strands pointing. Orange and ice blue rods represent the peptide stem and bridge structure, respectively. Bead A13 and A21 on the same stem are pointed out with arrows (both consist of a D-alanine) as well as A9 (L-alanine) on another stem. The distances between D-alanine and L-alanine from another stem are approximately 4-5 Å both.

The distances between several specified beads were studied in the following. As is announced by Kim et al.[10] and shown in figure 4, the distance between D-alanine and L-alanine from an adjacent stem is approximately 4 to 5 Å. Then the distances between these beads were measured by the use of the radial distribution function which was achieved by the *gmx_rdf* tool in GROMACS. They were compared to the reference data to verify whether they were consistent.

Water diffusion was calculated from the mean square displacement (MSD) of water beads for established systems with different cross-link percentages. It was achieved by the *gmx_msd* tool

in GROMACS. Three rates of cross-link that differ greatly were chosen for three very similar systems, 10%, 50% and 90%. Three small cubic volumes of water inside the PG structures were selected for which the diffusion coefficient were calculated by using linear regression. The average of the three groups was measured for each system and compared together.

CHAPTER 3

RESULTS AND DISCUSSION

3.1. Building PG Structures

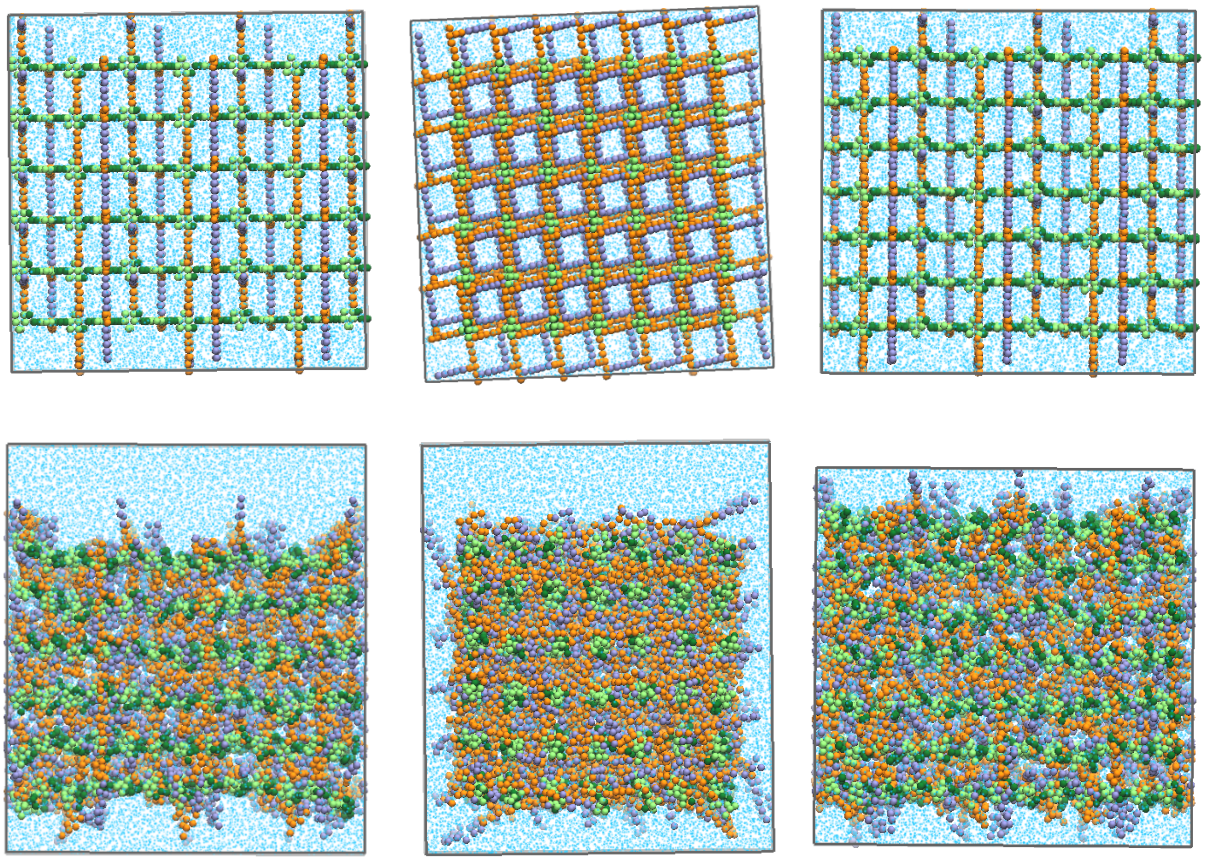

Figure 5. One example of PG structure generated by *PEPpy*. Front, side and top views are all shown in sequence. The configurations directly built by *PEPpy* are shown first, followed by the systems after 10 μs of NPT simulation. The three dimensions are 15nm×15nm×15nm.

The significant application of *PEPpy* is helping building different sizes of three dimensional cross-linked PG structures with specified percentage of cross-links as required. The dimension of the box received from users' input determines the carrying capacity of the system, where the width correlates with the length of glycan strands in particular. A typical example of PG solvated system generated with *PEPpy* is presented in figure 5. The initial structure built by *PEPpy* is shown first, followed by the corresponding configurations after a series of simulations. The top view and side views are both presented.

The three dimensions of the box for the large cubic PG structure were set to 15 nm each. Due to the specific size of a single unit, the actual size of the box could slightly deviate from the given *x, y, z* variables input by users. In this case, three dimensions were 14.1, 14.5 and 14.7 nm, respectively. The building process was complete within about 25 minutes. The whole structure consisted of 6 layers of PG with 7 glycan strands neatly arranged on a layer and each glycan stand was composed of 13 repeat units in the helical 4-fold axial symmetry. After a 10 μs NPT simulation which took approximately 164 hours to run when the energy minimization and NVT were done, the results were shown according to its original structure from front, side and top views.

Two different sizes of PG structures are shown below (figure 6). The long-strip type (figure 6a), 8, 8 and 20 nm for each dimension, was completed by *PEPpy* within 4 minutes. It contains 9 layers in height, 3 strands in one layer and 7 repeat units in one strand, and takes 68 hours to carry out whole MD simulations. The chunky type (figure 6b) measures approximately 14 nm long × 14 nm wide × 7 nm high. It takes 90 seconds to finish the construction by *PEPpy* and 52 hours through the complete simulation. Both results are shown in three perspectives.

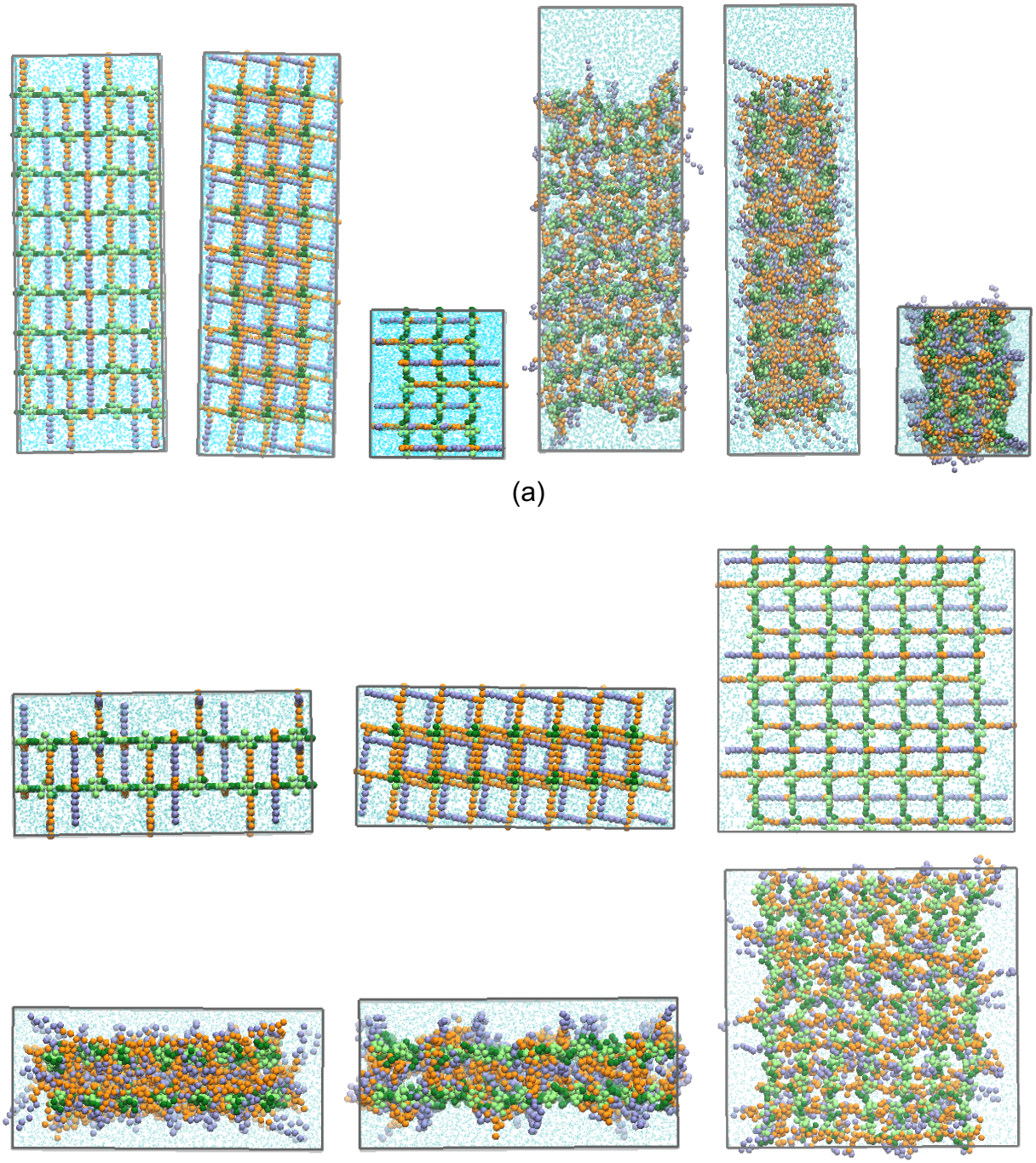

Figure 6. Another two examples generated by *PEPpy*. Front, side and top views are all shown in sequence. (a) 8nm×8nm×20nm. (b) 14nm×14nm×7nm

3.2 Validation of the PG Repeat Unit

Validation of the repeat unit was performed before building the whole structure in order that it was capable to replicate the behavior of the corresponding atomistic model. Achieved by PyCGTOOL, it compared bond lengths and angles between the CG and atomistic models after MD simulations. In order to achieve a small difference between atomistic and CG simulation results, a series of tests were performed to determine the constraints adding into the system. Bond lengths and angles listed in table 2 were achieved by processing the CG mapping through PyCGTOOL. Constraints were modified for each bond and angle respectively to narrow the gap between the two models after simulation to the greatest extent.

Table 2. Topological information of a CG repeat unit

Bond No.	Length (nm)	Constraint	Angle No.	Degree	Constraint
1-2	0.284	5000	1-2-3	127.4	100
2-3	0.314	5000	1-2-4	85.7	200
2-4	0.395	5000	3-2-4	81.9	200
4-5	0.314	5000	2-4-5	95.9	100
4-6	0.328	5000	2-4-6	154.7	100
4-8	0.335	5000	2-4-8	96.4	100
5-6	0.334	5000	5-4-8	164.5	100
6-7	0.304	5000	4-6-7	82.6	500
8-9	0.343	5000	6-4-8	106.3	100
9-10	0.365	5000	4-8-9	124.6	100
10-11	0.348	5000	5-6-7	114.2	100
11-12	0.341	5000	8-9-10	110.0	200
12-13	0.359	5000	9-10-11	90.2	100
12-14	0.344	5000	10-11-12	128.6	100
14-15	0.389	5000	11-12-13	104.7	100
15-16	0.306	5000	11-12-14	98.6	100
16-17	0.345	5000	13-12-14	133.3	100
17-18	0.456	5000	12-14-15	143.7	100
18-19	0.393	10000	14-15-16	129.6	100
19-20	0.356	5000	15-16-17	110.7	100
			16-17-18	131.7	100
			17-18-19	123.8	100
			18-19-20	121.1	100

In general, a percentage difference of bond lengths and angles between two compared models below 5% is considered acceptable. A series of factors such as the components of each bead, the bead type assigned and the connection methods may contribute to the differences. In table 3, most results (percentage difference) indicate a good match between the reference (atomistic) PG unit and CG mapping. However, several data are beyond the standard due to the trade-off in the large. Even a small change of one specific parameter would exert great influence in the whole mapping process. Therefore, after a comparison of over forty possible CG mappings, the one shown in table 3 was selected to be the most accurate representation of the reference structure. In addition, further validations were conducted to insure these deviations were acceptable.

Table 3. Percentage differences of bond lengths and angles between CG mapping and reference for the repeat unit after MD simulations.

Unit (20 beads)							
Bond Lengths				Angles			
Bonds	Ref	CG	%diff	Angles	Ref	CG	%diff
1-2	0.284 ± 0.008	0.281 ± 0.022	-1.12	1-2-3	130.8 ± 7.9	134.7 ± 8.5	3.84
2-3	0.312 ± 0.007	0.309 ± 0.021	-0.74	1-2-4	100.4 ± 6.1	102.1 ± 5.4	1.69
2-4	0.398 ± 0.009	0.398 ± 0.019	0.07	3-2-4	88.6 ± 9.1	97.2 ± 5.4	8.85
4-5	0.311 ± 0.014	0.309 ± 0.023	-0.80	2-4-5	93.9 ± 5.3	93.9 ± 6.4	-0.03
4-6	0.298 ± 0.005	0.300 ± 0.004	0.70	2-4-6	154.7 ± 5.6	148.8 ± 7.8	-5.87
4-8	0.312 ± 0.011	0.312 ± 0.021	-0.24	2-4-8	94.2 ± 6.6	94.5 ± 5.9	0.29
5-6	0.32 ± 0.010	0.316 ± 0.021	-0.96	5-4-8	161.6 ± 5.6	159.4 ± 6.9	-2.17
6-7	0.322 ± 0.017	0.32 ± 0.020	-0.38	4-6-7	92.3 ± 7.8	106.4 ± 8.4	14.08
8-9	0.352 ± 0.012	0.349 ± 0.024	-0.88	6-4-8	109.2 ± 5.6	112.2 ± 6.2	3.02
9-10	0.362 ± 0.018	0.359 ± 0.022	-0.86	4-8-9	112.9 ± 8.7	109.3 ± 8.8	-3.62
10-11	0.368 ± 0.024	0.365 ± 0.023	-0.73	5-6-7	139.4 ± 8.3	142.6 ± 8.0	3.14
11-12	0.346 ± 0.022	0.343 ± 0.023	-1.11	8-9-10	116.7 ± 9.3	113.5 ± 7.9	-3.23
12-13	0.337 ± 0.017	0.334 ± 0.024	-0.83	9-10-11	93.9 ± 10.6	97.0 ± 5.4	3.14
12-14	0.409 ± 0.016	0.406 ± 0.021	-0.83	10-11-12	147.6 ± 22.6	146.3 ± 9.7	-1.32
14-15	0.354 ± 0.019	0.352 ± 0.019	-0.63	11-12-13	106.1 ± 14.6	106.3 ± 8.3	0.23
15-16	0.401 ± 0.010	0.398 ± 0.019	-0.66	11-12-14	103.1 ± 14.0	105.0 ± 7.7	1.97
16-17	0.34 ± 0.022	0.336 ± 0.023	-1.18	13-12-14	97.8 ± 16.8	101.5 ± 8.4	3.72
17-18	0.338 ± 0.064	0.335 ± 0.017	-1.02	12-14-15	141.2 ± 14.7	139.3 ± 8.7	-1.88
18-19	0.338 ± 0.018	0.334 ± 0.022	-1.17	14-15-16	135.7 ± 16.3	135.1 ± 8.1	-0.56
19-20	0.353 ± 0.021	0.35 ± 0.021	-0.96	15-16-17	111.9 ± 19.0	112.8 ± 9.0	0.83
				16-17-18	123.0 ± 25.7	124.7 ± 8.7	1.65
				17-18-19	124.8 ± 12.8	125.9 ± 9.6	1.11
				18-19-20	119.7 ± 26.8	123.1 ± 8.2	3.37

Unit (21 beads)							
1-2	0.285 ± 0.007	0.268 ± 0.022	-6.09	1-2-3	129.4 ± 7.7	133.8 ± 8.7	3.47
2-3	0.315 ± 0.007	0.311 ± 0.021	-1.27	1-2-4	103.4 ± 10.9	104.5 ± 6.2	1.08
2-4	0.391 ± 0.013	0.395 ± 0.020	1.01	3-2-4	82.7 ± 9.7	88.0 ± 5.1	6.50
4-5	0.302 ± 0.014	0.298 ± 0.017	-1.58	2-4-5	95.7 ± 6.0	95.6 ± 6.1	-0.05
4-6	0.305 ± 0.006	0.333 ± 0.015	9.27	2-4-6	134.7 ± 6.8	134.6 ± 9.9	-0.08
4-8	0.351 ± 0.011	0.342 ± 0.017	-2.38	2-4-8	106.8 ± 7.8	102.5 ± 7.4	-4.10
5-6	0.341 ± 0.010	0.321 ± 0.025	-5.8	5-4-8	149.4 ± 7.0	149.5 ± 7.7	0.06
6-7	0.298 ± 0.012	0.316 ± 0.015	5.97	4-6-7	78.9 ± 5.8	88.3 ± 6.1	12.02
8-9	0.354 ± 0.015	0.345 ± 0.018	-2.59	6-4-8	105.5 ± 6.2	111.2 ± 6.8	5.50
9-10	0.365 ± 0.015	0.356 ± 0.024	-2.67	4-8-9	119.5 ± 14.4	119.8 ± 8.5	0.25
10-11	0.362 ± 0.024	0.351 ± 0.024	-3.03	5-6-7	123.6 ± 6.5	126.0 ± 8.2	2.03
11-12	0.355 ± 0.015	0.347 ± 0.023	-2.24	8-9-10	116.7 ± 9.9	113.6 ± 9.9	-2.66
12-13	0.354 ± 0.013	0.347 ± 0.022	-1.96	9-10-11	95.5 ± 10.7	96.8 ± 5.7	1.38
12-14	0.313 ± 0.015	0.309 ± 0.022	-1.24	10-11-12	129.5 ± 12.3	134.5 ± 9.1	3.91
14-15	0.295 ± 0.016	0.283 ± 0.021	-4.33	11-12-13	98.9 ± 8.0	101.2 ± 8.3	2.45
15-16	0.255 ± 0.011	0.248 ± 0.020	-2.85	11-12-14	95.4 ± 9.6	103.2 ± 8.1	8.18
16-17	0.34 ± 0.027	0.33 ± 0.022	-3.05	12-13-21	110.3 ± 10.5	107.3 ± 8.7	-2.75
17-18	0.361 ± 0.063	0.354 ± 0.017	-1.94	13-12-14	90.1 ± 8.0	98.2 ± 7.0	9.14
18-19	0.292 ± 0.019	0.283 ± 0.021	-3.08	12-14-15	152.9 ± 13.3	152.2 ± 8.6	-0.47
19-20	0.356 ± 0.021	0.369 ± 0.021	3.59	14-15-16	143.8 ± 15.6	144.3 ± 8.4	0.34
13-21	0.39 ± 0.011	0.376 ± 0.024	-3.69	15-16-17	122.9 ± 18.1	129.3 ± 8.6	5.26
				16-17-18	117.7 ± 25.9	117.8 ± 9.8	0.08
				17-18-19	140.1 ± 14.6	139.3 ± 9.1	-0.53
				18-19-20	119.1 ± 27.7	119.2 ± 8.1	0.10

3.3 Bonded parameters.

Bond lengths and angles were analyzed for the simulated PG structures after energy minimization, equilibrium and production MD simulation. Several typical frequency distributions of bond lengths and angles for the long strip type (figure 6a) are shown here (figure 7 and figure 8). Bond 1-2 and angle 1-2-3 are from the sugar head. Bond 10-11, 12-14, angle 8-9-10 and 11-12-14 are from the peptide stem. Bond 19-20 and angle 17-18-19 are from the

bridge structure. All the results of selected bond lengths and angles after the large time-scale simulations fall basically into a reasonable range and follow the Gaussian distribution.

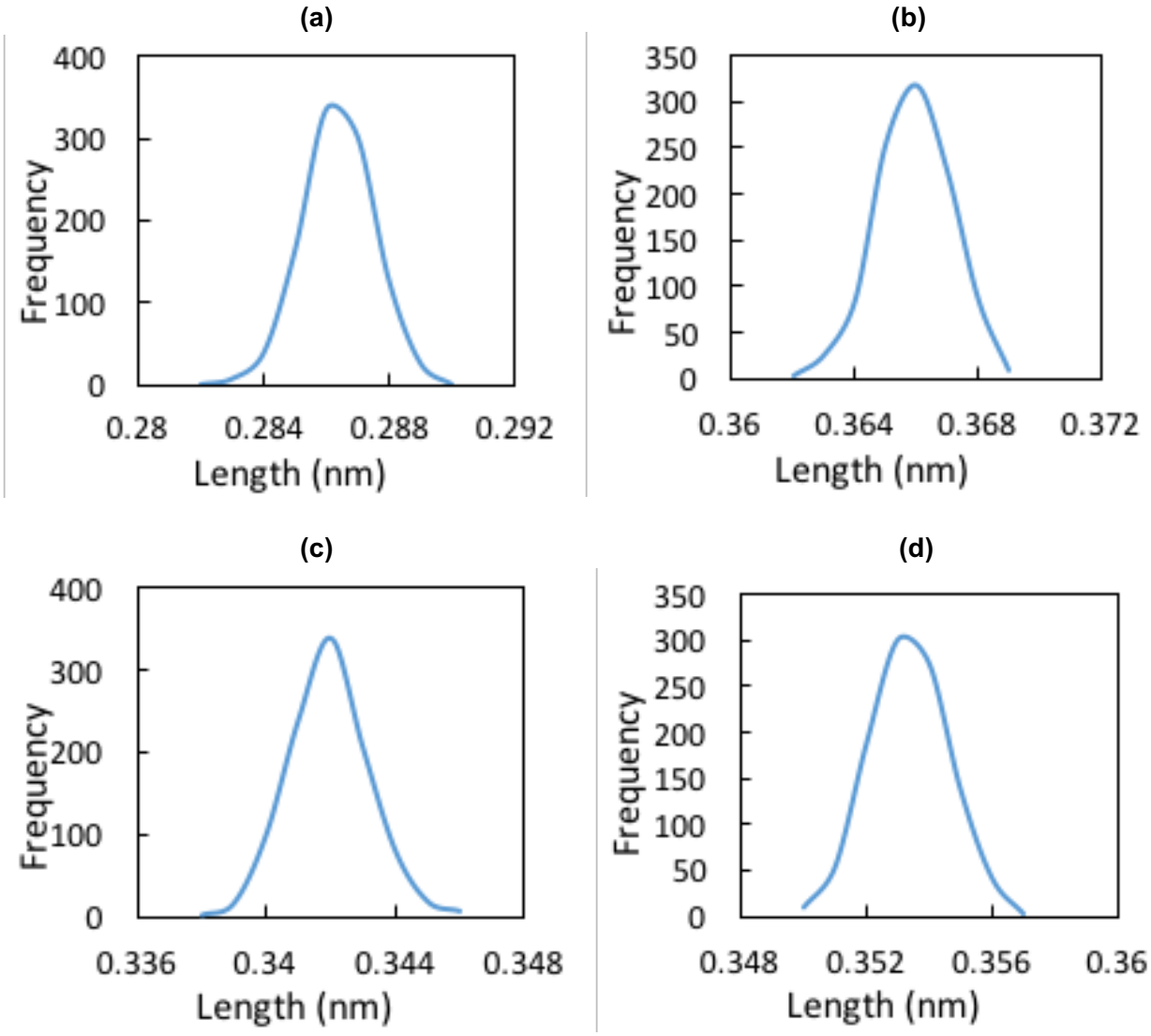

Figure 7. Bond length frequency distributions of peptidoglycan for bond (a)A1-A2, (b)A10-A11, (c)A12-A14 and (d)A19-A20.

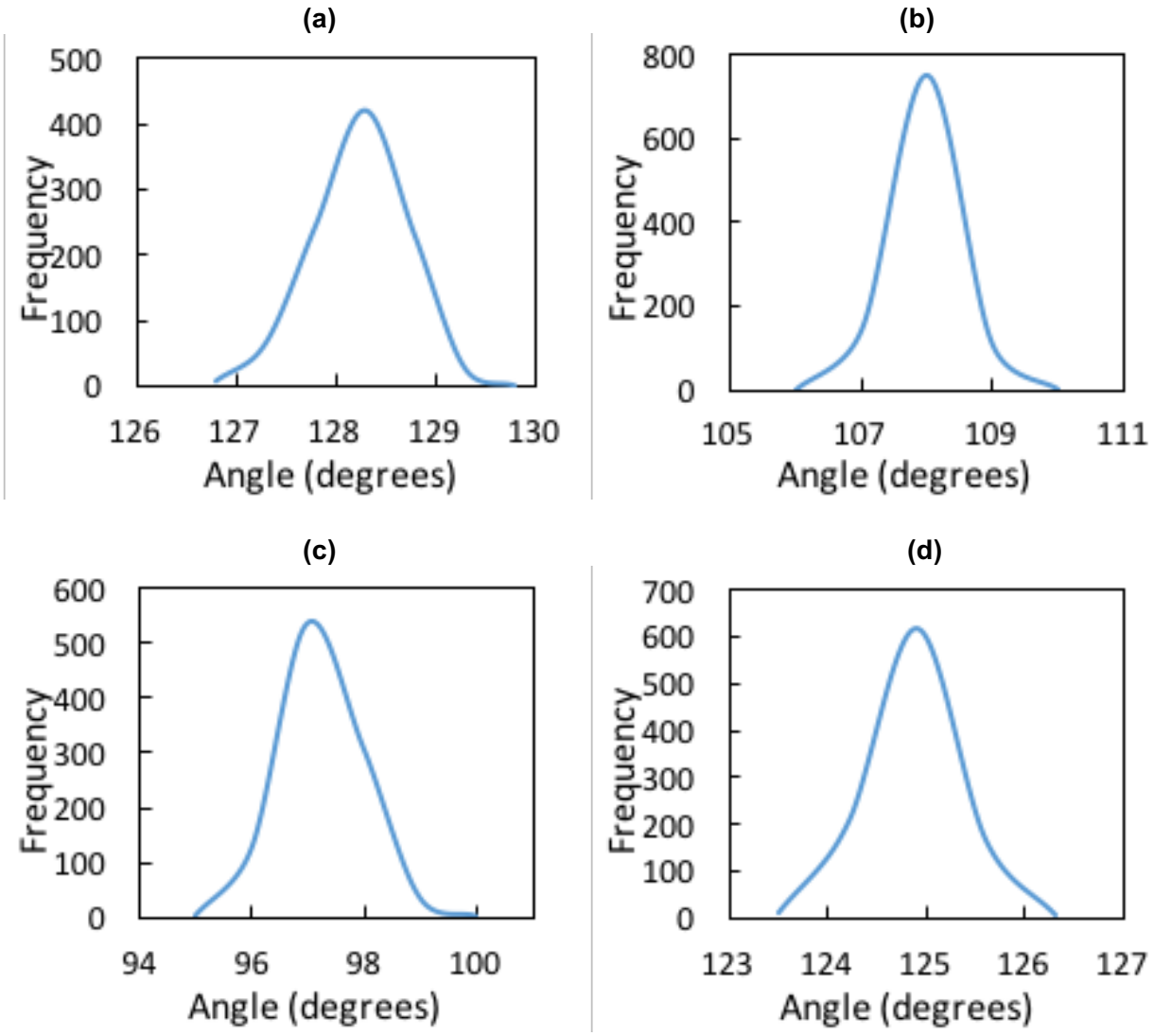

Figure 8. Bond angle frequency distributions of peptidoglycan for bond (a)A1-A2-A3, (b)A8-A9-A10, (c)A11-A12-A14 and (d)A17-A18-A19.

For bond lengths and angles each that are shown in the figure 7 and 8, comparisons are made between the CG structures before and after MD simulations (table 4). The parameters before MD simulations were obtained from the topological file (ITP file) of the PG repeat unit. Though the

lengths and angles of the bonds change along with time, the percentage differences between the two groups are quite small.

Table 4. Comparisons of bond lengths and angles between structures before and after MD simulations

Bond Lengths (nm)				
Bonds/Angles	Before MD	After MD	Std. Dev.	diff%
1-2	0.281	0.286	0.016	1.779
10-11	0.365	0.366	0.029	0.274
12-14	0.343	0.342	0.02	-0.291
19-20	0.350	0.353	0.021	0.857
Bond Angles (degree)				
1-2-3	127.42	128.50	0.46	0.848
8-9-10	109.99	108.47	0.45	1.386
11-12-14	98.61	97.51	0.66	1.111
17-18-19	123.85	125.21	0.44	1.102

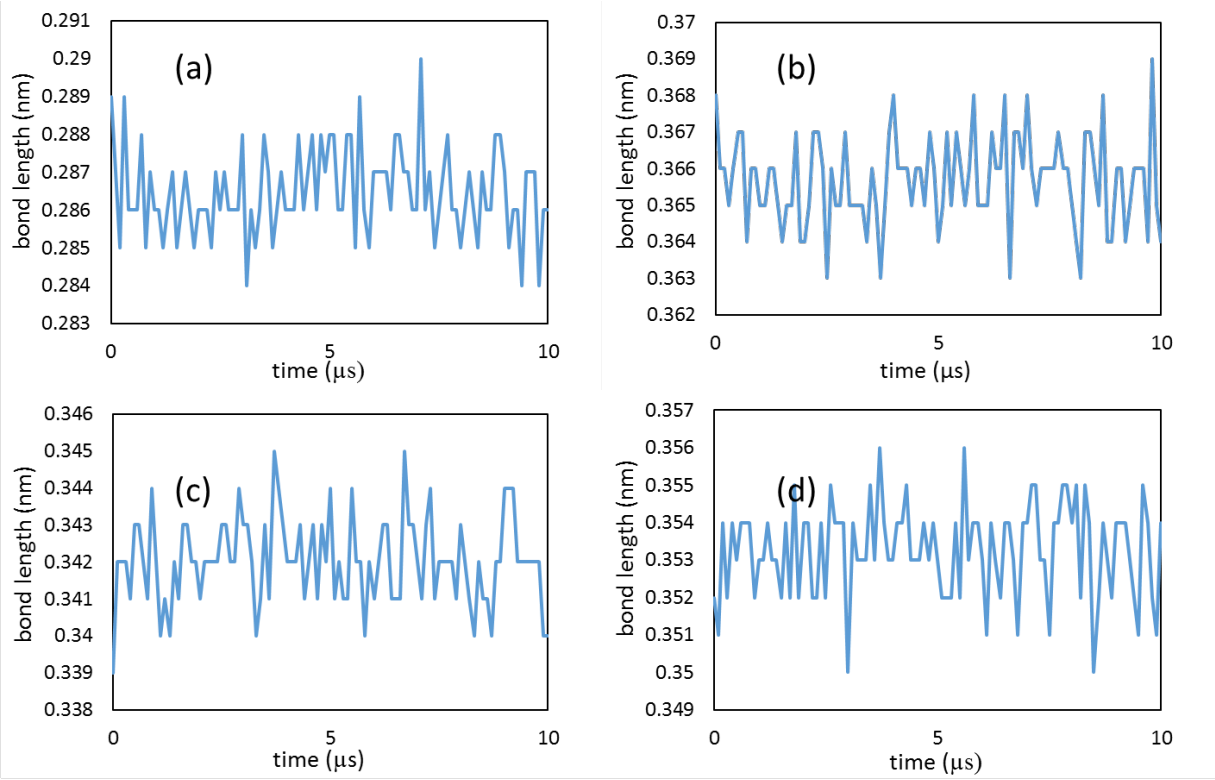

Figure 9. Bond lengths of (a)A1-A2, (b)A10-A11, (c)A12-A14 and (d)A19-A20 fluctuate with simulation time from 0 to 10μs.

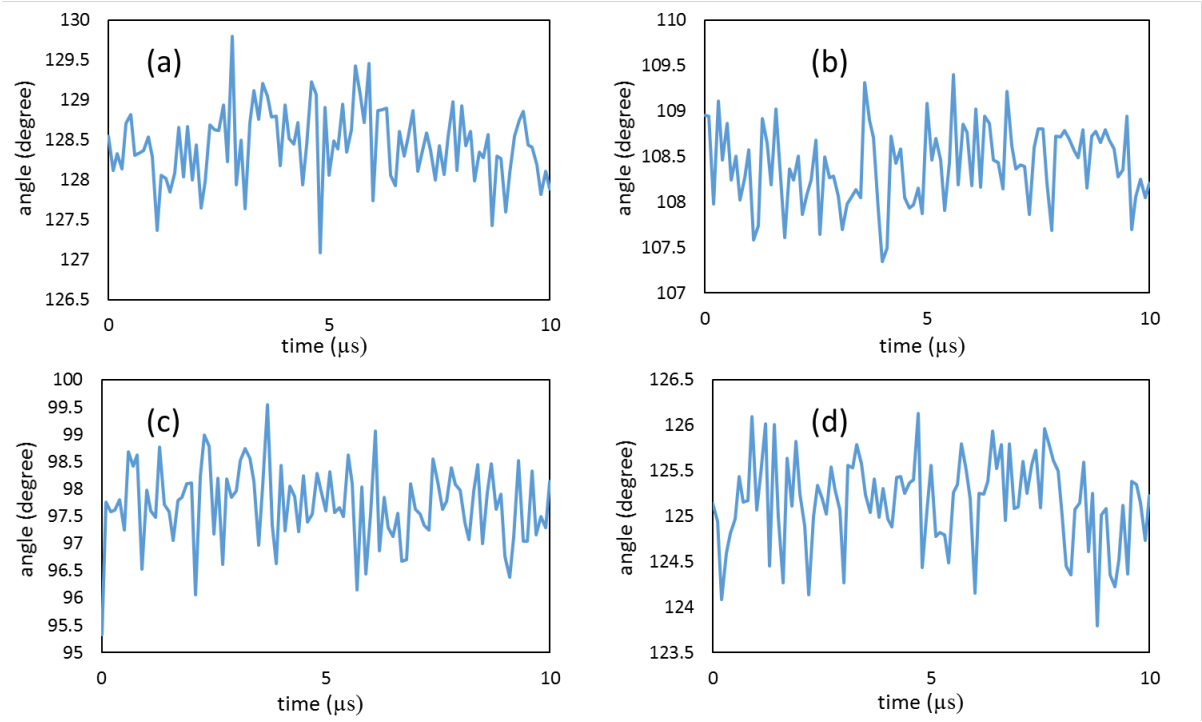

Figure 10. Several typical angles in the PG scaffold fluctuate with simulation time. (a)A1-A2-A3. (b)A8-A9-A10. (c)A11-A12-A14. (d)A17-A18-A19.

The behavior of the bonds and angles inside the PG scaffold through the whole Production MD simulation (NPT) was also studied. The relationship between the bond length and simulation time was depicted in figure 9 for the typical bonds mentioned before. Tendencies of the typical angles that varied with time were shown in figure 10. The bond lengths and angles fluctuated in a relatively small range around the specific values that correspond with the data in table 4. Therefore, it is confident to say the solvated PG scaffold would maintain well through the simulation.

3.4 Radial Distribution functions (RDF)

Announced by Kim et al. through isotope labelling method and rotational-echo double resonance NMR, a measured distance of approximately 4 to 5 Å could only be between the D-alanine from a unit stem in one glycan strand to the L-alanine from a unit of the adjacent glycan strand, since the intramolecular distance between the D-alanine and L-alanine on the same peptide stem have to be above 10 Å. Therefore, these distances can be measured for the coarse-grained PG structure built by the script to verify whether it can accurately replicate the atomistic structure.

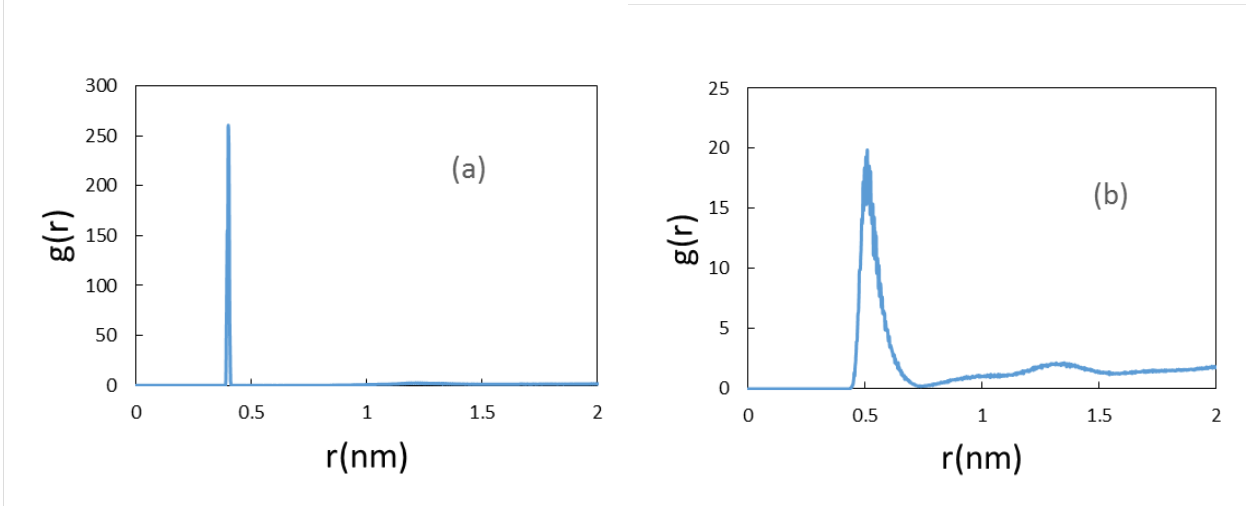

Figure 11. Radial distribution functions for (a) constrained interaction between A9 and A13 from adjacent PG units and (b) the interaction between A9 and A21 from adjacent PG units.

The validation was performed using radial distribution functions. The RDF in a system of particles such as atoms, molecules and coarse-grained beads describes the probability of finding a particle at distances from the selected reference particle, showing the density of the specified particle g(r) varies as a function of distance r. In this situation, ElNeDyn[47] was applied and a constraint called rubber band was added into the system. ElNeDyn stands for Elastic Network Dynamics. It is a method that utilize a set of springs or harmonic bonds to sustain the scaffold of

a structure. Therefore, “rubber bands” were added between the first D-alanine on the stem of a glycan strand (A13) and L-alanine (A9) from the unit of a neighboring glycan strand. The distance was set to 0.4 nm with a force constant of 500 $kJ\ mol^{-1}nm^{-2}$ to accord with the reference.

Then the distance between the edged D-alanine (A21) and L-alanine (A9) was measured using *RDF* commands in GROMACS. Results are shown in figure 11. Figure 11a is the RDF of the constrained interactions between the beads A9 and A13. It can be seen from figure 11a that the influence of the constraint is obvious due to the extreme height of the first peak. It means an extremely large percentage of the distances between A9 and A13 are exactly 0.4 nm in length. In figure 11b, it is shown that the first and highest peak of the curve g(r) is approximately located on 0.5 nm. Because no constraint was exerted between A9 and A21, the slope of the peak is more gentle compared to the peak in figure 7a. The second peak that locates on approximately 1.2 to 1.3 nm, which is smoother, may represent the distance between bead A9 and A21 from the same peptide stem. Therefore, the result is consistent with the reference.

3.5. Water diffusion in PG structures of different cross-link percentages.

Another property of the generated PG scaffold that I was interested in and tested is the water diffusion inside the solvated PG system. The diffusion coefficient of water in the system was measured for the simulated PG structures**.** Control variate method was adopted and three similar PG structures with same dimensions and water amount were built by *PEPpy* in succession. The three dimensions for each were 9, 7 and 9 nm with the only difference among them was the cross-link percentage for the three systems. 10%, 50% and 90% were set, respectively. Each

system was run for 5 μs under the pressure and temperature of 1 bar and 310 K. It took approximately 22 hours for each run to complete.

Table 5. Water diffusion coefficient of three PG systems with different cross-link rates. ($\times 10^{-5}$ cm^2/s)

cross-link rate	10%	50%	90%
group1	0.1912	0.1794	0.1725
group 2	0.1983	0.1761	0.1505
group 3	0.1964	0.1809	0.1657
average	0.1953	0.1788	0.1629

Three groups of water beads were chosen inside the PG structures to measure the diffusion coefficient. For each group, a 2×2×2 nm cubic box of water was selected and tested. All of the three groups were inside the built PG structure however were laid on different regions. The intention was to reduce the measurement error and avoid contingency factors. Results of the diffusion coefficient of water beads for PG system with different cross-link rates are listed in table 5. For each system, water diffusion coefficient will fluctuate a bit in a range, thus, an average is measured for each. The distribution coefficient decreases by 8.45% when the cross-link rate increases from 10% to 50%, and also decreases by 8.95% when the cross-link rate increases from 50% to 90%. Therefore, the tendency can be clearly observed from the table that under almost the same conditions, a negative correlation lies between the water diffusion coefficient and cross-link percentage in the PG structure. The finding is interesting yet this still needs the experimental data to validate and support.

CHAPTER 4

CONCLUSIONS AND FUTURE WORK

4.1 Conclusions

PEPpy is shown to enable the building of 3-dimensional bacterial PG scaffold effectively. By receiving the parameters including the three dimensions and cross-link percentage from the user's input, it is able to generate the desired PG system with specific cross-link rate and complete the solvation in the meantime. Due to the modeling at coarse-grained level, the PG systems are compatible with the Martini Force Field, making it possible to run MD simulations in larger time-scales for the complex systems so as to require the standard of characterization.

By performing a series of validations including the coarse-grained mapping validation, comparison of bonded parameters through the simulation and verification of the particular distances inside the structure, the PG scaffolds built by *PEPpy* are tested to be reliable for running MD simulations. In addition, the water diffusion test for the solvated PG systems suggests the relationship between the water diffusion coefficient and the cross-link percentage, that is, water beads diffuse faster in the scaffold with a lower cross-link rate.

4.2 Future Work

Future extensions of *PEPpy* include the generalization to the PG scaffolds of different bacterial species by modifying the PG unit chemical structure and the glycan strand arrangement. Additionally, the mosaic of proteins is another feature we plan to add into *PEPpy* in the future.

Since the bacterial outer membrane (Gram-negatives only) and inner cell membrane have been already well-modelled at the coarse-grained level, with the improvement of *PEPpy*, the intact bacterial cell envelopes are bound to be set up in the near future.

REFERENCES

1. Vollmer, W. and S.J. Seligman, *Architecture of peptidoglycan: more data and more models.* Trends in microbiology, 2010. **18**(2): p. 59-66.
2. Vollmer, W., D. Blanot, and M.A. De Pedro, *Peptidoglycan structure and architecture.* FEMS microbiology reviews, 2008. **32**(2): p. 149-167.
3. De Petris, S., *Ultrastructure of the cell wall of Escherichia coli and chemical nature of its constituent layers.* Journal of ultrastructure research, 1967. **19**(1-2): p. 45-83.
4. Murray, R., P. Steed, and H. Elson, *The location of the mucopeptide in sections of the cell wall of Escherichia coli and other gram-negative bacteria.* Canadian journal of microbiology, 1965. **11**(3): p. 547-560.
5. Silhavy, T.J., D. Kahne, and S. Walker, *The bacterial cell envelope.* Cold Spring Harbor perspectives in biology, 2010: p. a000414.
6. Labischinski, H., et al., *Direct proof of a" more-than-single-layered" peptidoglycan architecture of Escherichia coli W7: a neutron small-angle scattering study.* Journal of bacteriology, 1991. **173**(2): p. 751-756.
7. Dmitriev, B.A., et al., *Tertiary structure of Staphylococcus aureus cell wall murein.* Journal of bacteriology, 2004. **186**(21): p. 7141-7148.
8. Giesbrecht, P., et al., *Staphylococcal cell wall: morphogenesis and fatal variations in the presence of penicillin.* Microbiology and molecular biology reviews, 1998. **62**(4): p. 1371-1414.

9. Kim, S.J., J. Chang, and M. Singh, *Peptidoglycan architecture of Gram-positive bacteria by solid-state NMR.* Biochimica et Biophysica Acta (BBA)-Biomembranes, 2015. **1848**(1): p. 350-362.

10. Kim, S.J., et al., *Staphylococcus aureus peptidoglycan stem packing by rotational-echo double resonance NMR spectroscopy.* Biochemistry, 2013. **52**(21): p. 3651-3659.

11. Navarre, W.W. and O. Schneewind, *Surface proteins of gram-positive bacteria and mechanisms of their targeting to the cell wall envelope.* Microbiology and molecular biology reviews, 1999. **63**(1): p. 174-229.

12. Kimura, K.-i. and T.D. Bugg, *Recent advances in antimicrobial nucleoside antibiotics targeting cell wall biosynthesis.* Natural product reports, 2003. **20**(2): p. 252-273.

13. Lovering, A.L., S.S. Safadi, and N.C. Strynadka, *Structural perspective of peptidoglycan biosynthesis and assembly.* Annual review of biochemistry, 2012. **81**: p. 451-478.

14. Beeby, M., et al., *Architecture and assembly of the G ram-positive cell wall.* Molecular microbiology, 2013. **88**(4): p. 664-672.

15. Gan, L., S. Chen, and G.J. Jensen, *Molecular organization of Gram-negative peptidoglycan.* Proceedings of the National Academy of Sciences, 2008. **105**(48): p. 18953-18957.

16. Turner, R.D., et al., *Peptidoglycan architecture can specify division planes in Staphylococcus aureus.* Nature communications, 2010. **1**: p. 26.

17. Turner, R.D., et al., *Cell wall elongation mode in Gram-negative bacteria is determined by peptidoglycan architecture.* Nature communications, 2013. **4**: p. 1496.

18. Bond, P.J., et al., *Coarse-grained molecular dynamics simulations of membrane proteins and peptides.* Journal of structural biology, 2007. **157**(3): p. 593-605.

19. Piggot, T.J., D.A. Holdbrook, and S. Khalid, *Electroporation of the E. coli and S. aureus membranes: molecular dynamics simulations of complex bacterial membranes.* The Journal of Physical Chemistry B, 2011. **115**(45): p. 13381-13388.

20. Ma, H., et al., *Modeling diversity in structures of bacterial outer membrane lipids.* Journal of chemical theory and computation, 2017. **13**(2): p. 811-824.

21. Ma, H., et al., *Simulating Gram-negative bacterial outer membrane: a coarse grain model.* The Journal of Physical Chemistry B, 2015. **119**(46): p. 14668-14682.

22. Ma, H., A. Khan, and S. Nangia, *Dynamics of OmpF trimer formation in the bacterial outer membrane of Escherichia coli.* Langmuir, 2017. **34**(19): p. 5623-5634.

23. Gumbart, J.C., et al., *Escherichia coli peptidoglycan structure and mechanics as predicted by atomic-scale simulations.* PLoS computational biology, 2014. **10**(2): p. e1003475.

24. Samsudin, F., et al., *Braun's Lipoprotein Facilitates OmpA Interaction with the Escherichia coli Cell Wall.* Biophysical journal, 2017. **113**(7): p. 1496-1504.

25. Khalid, S., T.J. Piggot, and F. Samsudin, *Atomistic and Coarse Grain Simulations of the Cell Envelope of Gram-Negative Bacteria: What Have We Learned?* Accounts of chemical research, 2018.

26. Marrink, S.J., et al., *The MARTINI force field: coarse grained model for biomolecular simulations.* The journal of physical chemistry B, 2007. **111**(27): p. 7812-7824.

27. Marrink, S.J., A.H. De Vries, and A.E. Mark, *Coarse grained model for semiquantitative lipid simulations.* The Journal of Physical Chemistry B, 2004. **108**(2): p. 750-760.

28. Shih, A.Y., et al., *Coarse grained protein− lipid model with application to lipoprotein particles.* The Journal of Physical Chemistry B, 2006. **110**(8): p. 3674-3684.

29. Stevens, M.J., *Coarse-grained simulations of lipid bilayers.* The Journal of chemical physics, 2004. **121**(23): p. 11942-11948.

30. Müller, M., K. Katsov, and M. Schick, *Biological and synthetic membranes: What can be learned from a coarse-grained description?* Physics Reports, 2006. **434**(5-6): p. 113-176.

31. Tozzini, V., *Coarse-grained models for proteins.* Current opinion in structural biology, 2005. **15**(2): p. 144-150.

32. Neri, M., et al., *Coarse-grained model of proteins incorporating atomistic detail of the active site.* Physical review letters, 2005. **95**(21): p. 218102.

33. Monticelli, L., et al., *The MARTINI coarse-grained force field: extension to proteins.* Journal of chemical theory and computation, 2008. **4**(5): p. 819-834.

34. Schüttelkopf, A.W. and D.M. Van Aalten, *PRODRG: a tool for high-throughput crystallography of protein–ligand complexes.* Acta Crystallographica Section D: Biological Crystallography, 2004. **60**(8): p. 1355-1363.

35. Van Der Spoel, D., et al., *GROMACS: fast, flexible, and free.* Journal of computational chemistry, 2005. **26**(16): p. 1701-1718.

36. Hess, B., et al., *GROMACS 4: algorithms for highly efficient, load-balanced, and scalable molecular simulation.* Journal of chemical theory and computation, 2008. **4**(3): p. 435-447.

37. Abraham, M.J., et al., *GROMACS: High performance molecular simulations through multi-level parallelism from laptops to supercomputers.* SoftwareX, 2015. **1**: p. 19-25.

38. Cornell, W.D., et al., *A second generation force field for the simulation of proteins, nucleic acids, and organic molecules.* Journal of the American Chemical Society, 1995. **117**(19): p. 5179-5197.

39. van Gunsteren, W.F., X. Daura, and A.E. Mark, *GROMOS force field.* Encyclopedia of computational chemistry, 2002. **2**.

40. Schmid, N., et al., *Definition and testing of the GROMOS force-field versions 54A7 and 54B7.* European biophysics journal, 2011. **40**(7): p. 843.

41. Marrink, S.J., et al., *Computational Modeling of Realistic Cell Membranes.* Chemical reviews, 2019.

42. Lafon, S. and A.B. Lee, *Diffusion maps and coarse-graining: A unified framework for dimensionality reduction, graph partitioning, and data set parameterization.* IEEE transactions on pattern analysis and machine intelligence, 2006. **28**(9): p. 1393-1403.

43. Nielsen, S.O., et al., *Coarse grain models and the computer simulation of soft materials.* Journal of Physics: Condensed Matter, 2004. **16**(15): p. R481.

44. Bradley, R. and R. Radhakrishnan, *Coarse-grained models for protein-cell membrane interactions.* Polymers, 2013. **5**(3): p. 890-936.

45. Graham, J.A., J.W. Essex, and S. Khalid, *PyCGTOOL: automated generation of coarse-grained molecular dynamics models from atomistic trajectories.* Journal of chemical information and modeling, 2017. **57**(4): p. 650-656.

46. Wassenaar, T.A., et al., *Computational lipidomics with insane: a versatile tool for generating custom membranes for molecular simulations.* Journal of chemical theory and computation, 2015. **11**(5): p. 2144-2155.

47. Periole, X., et al., *Combining an elastic network with a coarse-grained molecular force field: structure, dynamics, and intermolecular recognition.* Journal of Chemical Theory and Computation, 2009. **5**(9): p. 2531-2543.

VITA

Xichen Xu was born and raised in Jinhua, China, where he attended the primary school and high school till 2012. He continued his education at the University of Science and Technology of China and majored in materials chemistry, where he worked with Professor Chunhua Chen in the field of lithium battery. After earning his Bachelor of Science in Materials Chemistry at U.S.T.C. in July, 2016, Xichen decided to pursue a master's degree in the USA. He began graduate school at Syracuse University in August 2016 and majored in Chemical Engineering. He joined Professor Shikha Nangia's research group since 2017 and is currently working on the project of using a tool to generate bacterial peptidoglycan scaffolds for molecular dynamics simulations.